Chemical Science

ROYAL SOCIETY OF CHEMISTRY

EDGE ARTICLE

View Article Online
View Journal | View Issue

Cite this: *Chem. Sci.*, 2022, **13**, 8679

All publication charges for this article have been paid for by the Royal Society of Chemistry

Received 5th May 2022
Accepted 5th July 2022

DOI: 10.1039/d2sc02503e

rsc.li/chemical-science

Phenothiazine-based covalent organic frameworks with low exciton binding energies for photocatalysis†

Weitao Wang,‡[a] Haotian Wang,‡[a] Xiaohui Tang,[a] Jinlei Huo,[a] Yan Su,[a] Chuangye Lu,[a] Yujian Zhang,*[c] Hong Xu*[b] and Cheng Gu*[ad]

Designing delocalized excitons with low binding energy (E_b) in organic semiconductors is urgently required for efficient photochemistry because the excitons in most organic materials are localized with a high E_b of >300 meV. In this work, we report the achievement of a low E_b of ~50 meV by constructing phenothiazine-based covalent organic frameworks (COFs) with inherent crystallinity, porosity, chemical robustness, and feasibility of bandgap engineering. The low E_b facilitates effective exciton dissociation and thus promotes photocatalysis by using these COFs. As a demonstration, we subject these COFs to photocatalytic polymerization to synthesize polymers with remarkably high molecular weight without any requirement of the metal catalyst. Our results can facilitate the rational design of porous materials with low E_b for efficient photocatalysis.

Introduction

Photocatalysis is a kind of multi-step redox reaction triggered/promoted by light energy, in which the dissociation of light-induced excitons plays a key role in forming free electrons and holes that react with substrates to achieve various catalytic reactions, such as water splitting,[1] CO_2 reduction,[2] organic synthesis,[3] and polymerization.[4] Recent advances have extensive achievements in materials design, bandgap engineering, and catalytic optimization. However, there are rare reports on manipulating the exciton dissociation process. The exciton binding energy (E_b) has been regarded as a crucial parameter for mediating charge separation in photochemistry. Generally, in inorganic semiconductors such as GaN, perovskite, and MoS_2, the excitons are delocalized Wannier excitons with an ultralow E_b of <25 meV,[5–9] which means that the excitons spontaneously dissociate into free electrons and holes at room temperature, facilitating their photochemistry by promoted exciton utilization. By contrast, in organic small-molecule and polymer materials, the excitons are localized Frank excitons, with an E_b as high as >300 meV.[10,11] It is quite difficult to achieve efficient exciton dissociation and long-range migration, which has become the bottleneck issue for photocatalysis by using organic materials.[12–14] There are several examples for reducing the E_b to <100 meV in organic single crystals[15] and polymers.[16,17] However, neither rational design nor function-led syntheses that enable such low E_b systems, in which the relationship of the structures, the E_b, and the photofunctions are required to be predesigned with molecular-level precision, have been proposed so far. Therefore, manipulating the E_b of organic semiconductors to a substantially low value for promoted photochemistry is highly desired in this field but remains a challenge.

An established strategy to reduce the E_b is incorporating a strong donor (D) and strong acceptor (A) into one molecule to promote charge separation, which was demonstrated to be effective in polymer solar cell systems.[18] On the other hand, assembling D–A molecules into crystalline solids can amplify the charge separation and long-range charge transport *via* the through-space interactions in the well-defined crystalline lattice.[19,20] Particularly, covalent organic frameworks (COFs) are an emerging class of crystalline porous polymers that allow the atomically precise integration of desirable π units to create predesigned skeletons and nanopores,[21] and their unique features of well-defined crystalline porous structure, and high stability together with tailored functionality make them promising materials for photocatalysis.[22] However, the construction of low-E_b COFs is still very difficult. This is because, compared

[a]*State Key Laboratory of Luminescent Materials and Devices, Institute of Polymer Optoelectronic Materials and Devices, South China University of Technology, No. 381 Wushan Road, Tianhe District, Guangzhou 510640, P. R. China. E-mail: gucheng@scut.edu.cn*

[b]*Institute of Nuclear and New Energy Technology, Tsinghua University, Beijing, 100084, P. R. China. E-mail: hongxu@tsinghua.edu.cn*

[c]*Department of Chemistry, Zhejiang Normal University, Jinhua 321004, P. R. China. E-mail: sciencezyj@foxmail.com*

[d]*Guangdong Provincial Key Laboratory of Luminescence from Molecular Aggregates, South China University of Technology, No. 381 Wushan Road, Tianhe District, Guangzhou, 510640, P. R. China*

† Electronic supplementary information (ESI) available. See https://doi.org/10.1039/d2sc02503e

‡ These authors contributed equally to this work.

to linear organic polymers that could be readily synthesized by various synthetic reactions, crystallizing the π units into the COF lattice is still challenging,[23,24] although several building blocks including perylene bisimide,[25] porphyrin,[26] dibenzochrysene,[27] and isoindigo[28] have been encoded into frameworks while maintaining their crystallinity.[29] For instance, phenothiazine is a S, N atom-fused polycyclic aromatic molecule with a butterfly-shaped configuration. The dihedral angle of the two benzene rings could vary from 120° to 180° in response to the stimuli of the external environment.[30] On the other hand, phenothiazine possesses a considerably high highest occupied molecular orbital (HOMO) energy level of about −5.0 eV, which reveals a strong donor feature and thus allows phenothiazine in various applications such as light emission,[30] dye-sensitized solar cells,[31] and photocatalysis.[32] However, such a useful donor unit has not yet been reported to construct COFs because the butterfly shape and variable configuration impede the crystallization of phenothiazine-based COFs.

In this report, we for the first time constructed phenothiazine-based, crystalline, and porous two-dimensional (2D) and one-dimensional (1D) COFs with a 10-methylphenothiazine-3,7-dicarbaldehyde (MPTz) building block reacting with diverse amino or acetonitrile monomers by imine- or acrylonitrile-bond formation under acidic or basic conditions. The resulting COFs offer a platform for intensive investigation of E_b manipulation by changing the acceptor building blocks, yielding low E_b values of 50 meV in COFs. We demonstrated the utility of these photoactive COFs by subjecting them to photocatalytic polymerization to synthesize polymers with remarkably high molecular weight without any additional metal catalyst, thus providing a new prospect for developing low-E_b photocatalytic crystalline organic materials.

Results and discussion

The phenothiazine-based COFs were synthesized by linking electron-donor unit MPTz to different acceptor units, 1,3,5-tris(4-aminophenyl)benzene (TAPB), benzene-1,3,5-triyltriacetonitrile (BTTA), and 1,3,6,8-tetra(4-aminophenyl) pyrene (TAPP), respectively (Fig. 1a). Note that TAPB and TAPP are commonly recognized as electron-donor moieties;[33,34] however, because of the sufficiently strong electron-donating property and much higher HOMO energy level of phenothiazine, TAPB and TAPP become electron acceptors when linking with the MPTz unit. We screened various synthetic conditions including solvent, temperature, and reaction time (Table S1†), and obtained three crystalline frameworks, termed PTz-TPB-COF, PTz-BTA-COF, and PTz-Py-COF, in the presence of acid or base at 120 °C for 3 d (Fig. 1a). Remarkably, the crystallinity of these COFs (Fig. 2a–c) was achieved both in imine-bond formation and Knoevenagel condensation reactions, demonstrating the adaptation of the phenothiazine building block in reaction versatility. The chemical structures were characterized by various analytical methods. PTz-TPB-COF showed the absence of amino stretching vibration peaks at 3434 cm^{-1} and 3355 cm^{-1}, absence of the carbonyl stretching vibration peak at

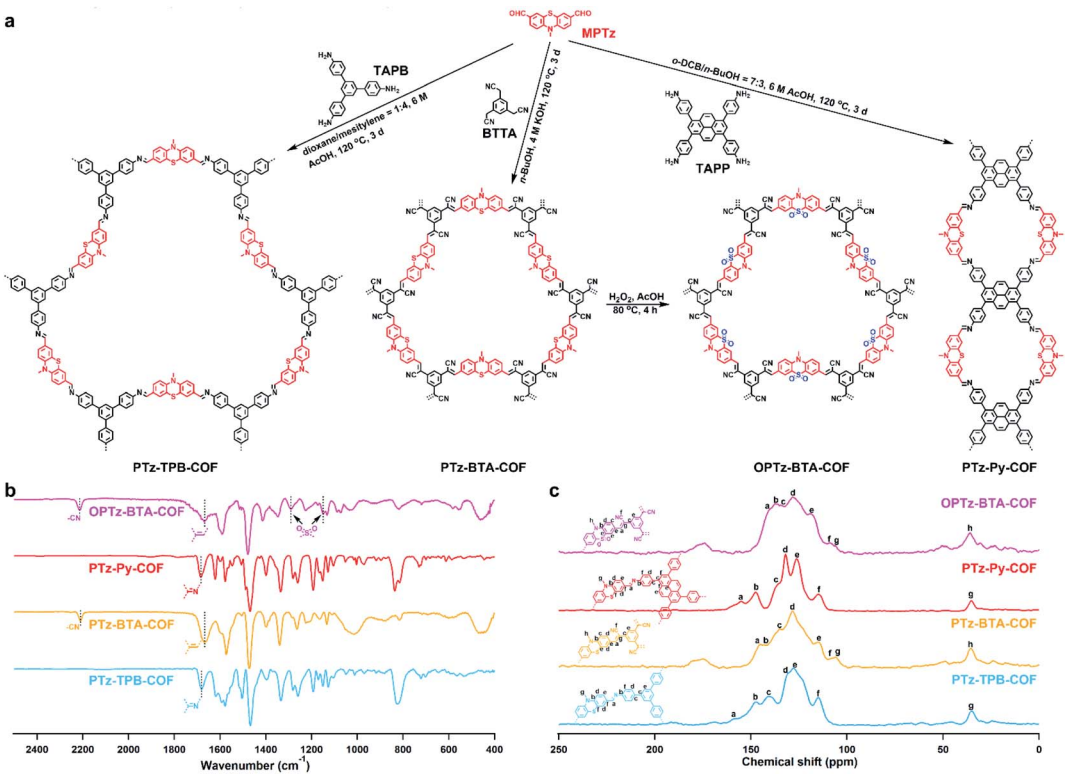

Fig. 1 (a) Synthesis of phenothiazine-based COFs. (b) FT-IR spectra of PTz-TPB-COF, PTz-BTA-COF, PTz-Py-COF, and OPTz-BTA-COF. (c) Solid-state ^{13}C NMR spectra of PTz-TPB-COF, PTz-BTA-COF, PTz-Py-COF, and OPTz-BTA-COF.

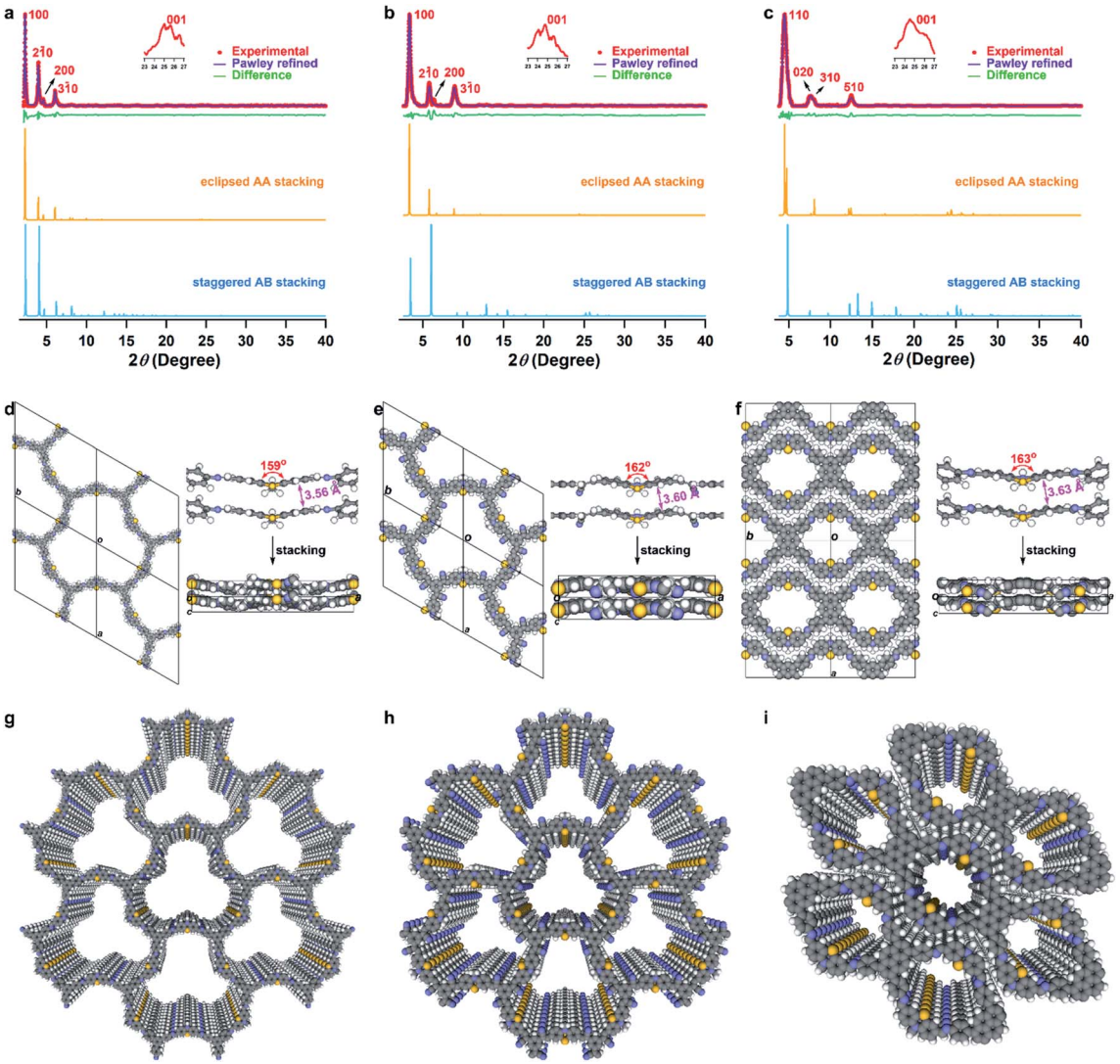

Fig. 2 (a), (b) and (c) Experimental and simulated PXRD patterns of PTz-TPB-COF, PTz-BTA-COF, and PTz-Py-COF, respectively. (d), (e) and (f) Top and side views of the unit cells in eclipsed stacking mode. The dihedral angles of the two benzene rings in phenothiazine moieties and the π–π distance of the two layers are also provided. Color code: H, white; C, gray; N; blue; S, yellow. (g), (h) and (i) Graphic views of eclipsed AA stacking structures of the three COFs.

1679 cm^{-1}, and occurrence of the C=N stretching vibration peak at 1682 cm^{-1} in the infrared spectrum (Fig. 1b, S1 and Table S2†). Solid-state ^{13}C NMR of PTz-TPB-COF revealed the presence of peaks at 35 and 143 ppm, which were attributed to the carbons on methyl and phenothiazine (9a and 10a position), respectively (Fig. 1c and Table S3†). Elemental analysis performed on the guest-free PTz-TPB-COF was in good agreement with the expected formula (Table S4†). Similarly, the structure and components of PTz-BTA-COF and PTz-Py-COF could also be fully assigned (Fig. 1b, c, S2, S3 and Tables S2–S4†). Because the S atom in the phenothiazine unit could be readily oxidized and yield the phenothiazine 5,5-dioxide moiety,[35] we treated PTz-BTA-COF with H_2O_2 and acetic acid and obtained a new framework, termed OPTz-BTA-COF. IR spectra revealed two newly generated peaks at 1148 and 1290 cm^{-1}, which were attributed to the stretching vibration of the S=O bond, whereas the other parts of COFs remained unchanged (Fig. 1b, Tables S2 and S4†). Solid-state ^{13}C NMR spectra showed that the oxidation apparently changed the chemical shifts of the carbon atoms at the *a*, *b*, and *e* positions (Fig. 1c, Tables S3 and S4†), whereas the positions of the other carbon atoms kept unchanged. On the other hand, the imine bonds in PTz-TPB-COF and PTz-Py-COF underwent oxidation and decomposition when treated with H_2O_2 and acetic acid (Fig. S4 and S5†).

Scanning electron microscopy (SEM) confirmed only one morphology for each COF, indicating their phase purity (Fig. S6†). Transmission electron microscopy (TEM) of synthesized COFs showed thin layer structures, and high-resolution TEM and selected-area electron diffraction (SAED) further showed the presence of porous textures that produced clear diffraction patterns (Fig. S7†). The crystallinity was confirmed by powder X-ray diffraction (PXRD), with no diffraction peaks

attributable to the starting materials (Fig. S8†). The PXRD pattern of the PTz-TPB-COF revealed several obvious peaks at $2\theta = 2.29°$, 3.98°, 4.55°, and 25.05°, corresponding to (100), (2$\bar{1}$0), (200), and (001) reflection planes (Fig. 2a). To determine the crystal structures, crystal models were generated based on the geometry of the building blocks. The optimal cell length was $a = b = 44.6434$ Å, $c = 3.7300$ Å, $\alpha = \beta = 90°$, $\gamma = 120°$ (Fig. 2d and Table S5†). Likewise, the unit cell parameters of PTz-BTA-COF can also be obtained by simulations (Fig. 2b and e, Tables S7 and S9†). Using the structures of the monolayers, two stacked configurations for each COF, that is, eclipsed AA and staggered AB modes, were generated and optimized (Fig. 2a–c, S9 and Tables S5–S10†). It is noteworthy that due to the limited number of peaks, it is not possible to unambiguously assign the framework to either the eclipsed or staggered stacking mode.[36] However, the porosity data facilitate the differentiation of these two modes (*vide infra*). Interestingly, PTz-Py-COF adopted a dense stacking of the 1D framework, which is different from other pyrene-based COFs with 2D frameworks. This could be distinguished from their experimental and simulated PXRD patterns (Fig. 2c, f, i, S9, Tables S9 and S10†). The simulated PXRD pattern of the eclipsed AA model was in good agreement with the experimental pattern, which confirmed that PTz-Py-COF adopted an eclipsed AA stacking arrangement (Fig. 2c). Notably, the phenothiazine moieties in all three COFs adopted the butterfly configuration, with dihedral angles from 159° to 163° for the two benzene rings, while the π–π distances of the two layers were 3.56, 3.60, and 3.63 Å for PTz-TPB-COF, PTz-BTA-COF, and PTz-Py-COF, respectively (Fig. 2d–f). These were enlarged compared to the common COFs with a layer distance of 3.3 to 3.4 Å (ref. 37) thus indicating weak interlayer interactions and resulting in wavy frameworks (Fig. 2d–f) with loose stacking. On the other hand, OPTz-BTA-COF retained the crystallinity upon oxidation (Fig. S10†).

The porosity of PTz-TPB-COF, PTz-BTA-COF, PTz-Py-COF, and OPTz-BTA-COF was characterized by N_2 adsorption at 77 K by using activated samples. The isotherm of PTz-TPB-COF showed a type IV shape, and the isotherm of PTz-Py-COF revealed a type I shape, whereas isotherms of PTz-BTA-COF and OPTz-BTA-COF exhibited the combination of two uptake trends in the relative pressures of $P/P_0 < 0.01$ and $0.01 < P/P_0 < 0.1$ (Fig. S11†), indicating the mesoporosity of PTz-TPB-COF, PTz-BTA-COF, and OPTz-BTA-COF, and the microporosity of PTz-Py-COF. Brunauer–Emmett–Teller (BET) surface areas were calculated to be 236.6, 535.8, 540.9, and 529.5 $m^2\ g^{-1}$ for PTz-TPB-COF, PTz-BTA-COF, PTz-Py-COF, and OPTz-BTA-COF, respectively (Fig. S12†). The pore-size distributions were estimated to be 4.52, 2.37, 1.20, and 2.32 nm (Fig. S13†), which were in good agreement with the eclipsed AA models and further confirmed that the four COFs adopted eclipsed AA stacking arrangements. These results demonstrated that all four COFs are highly porous with large surface areas.

The thermal stability of PTz-TPB-COF, PTz-BTA-COF, and PTz-Py-COF was evaluated using thermogravimetric analysis (TGA). The three COFs were thermally stable up to 200 °C under a N_2 atmosphere (Fig. S14†), whereas from 200 to 300 °C, they lost the $-CH_3$ moieties on the phenothiazine groups. For PTz-BTA-COF, the continuous weight loss from 300 to 500 °C was because of the removal of the –CN groups from its skeleton. The chemical stability of PTz-TPB-COF, PTz-BTA-COF, and PTz-Py-COF was checked by immersing the COFs into concentrated HCl or NaOH solutions at room temperature. PXRD patterns and N_2 adsorption analysis before and after immersion for 3 d revealed almost no change in crystallinity and porosity (Fig. S15 and S16†), demonstrating the long-term integrity of the frameworks.

The bandgaps of the COFs were initially evaluated by the UV-vis diffuse reflectance spectra measurements, which revealed that the absorption edges were at 578, 621, 562, and 505 nm for PTz-TPB-COF, PTz-BTA-COF, PTz-Py-COF, and OPTz-BTA-COF, respectively (Fig. S17a†), corresponding to the optical bandgaps of 2.29, 2.09, 2.28, and 2.55 eV (Fig. S17b†). Notably, PTz-BTA-COF exhibited a substantially narrowed bandgap compared to PTz-TPB-COF and PTz-Py-COF, which originates from the enhanced π-conjugated D–A structures by acrylonitrile-bond formation where BTTA acts as a strong electron acceptor. On the other hand, the bandgap of OPTz-BTA-COF was obviously enlarged compared to that of PTz-BTA-COF, indicating that manipulating S oxidation states effectively regulated the bandgap of the COFs. We further assessed the HOMO/LUMO energy levels by differential pulse voltammetry (DPV) tests (Fig. S18†), which showed a characteristically oxidative wave at a very low potential of 0.3 V at the positive position for PTz-TPB-COF, PTz-BTA-COF, and PTz-Py-COF, revealing the strong electron-donating ability and high HOMO position of the phenothiazine moiety. The HOMO/LUMO energy levels for PTz-TPB-COF, PTz-BTA-COF, PTz-Py-COF, and OPTz-BTA-COF were −5.05/−2.75, −5.20/−3.04, −5.04/−2.86, and −5.27/−2.68 eV, calculated from the onset of the first redox peaks (Fig. S19†). Thus, the electrochemical bandgaps were 2.30, 2.16, 2.18, and 2.59 eV, respectively, which matched well with the optical bandgaps. Notably, OPTz-BTA-COF possessed an obviously decreased HOMO level and increased LUMO level compared to that of PTz-BTA-COF, showing that phenothiazine 5,5-dioxide became a weak electron donor.

All these COFs exhibited photoluminescence properties; orange ($\lambda_{max} = 582$ nm, photoluminescence quantum yield (PLQY) = 1.1%), red ($\lambda_{max} = 660$ nm, PLQY = 6.7%), yellow ($\lambda_{max} = 566$ nm, PLQY = 1.4%) and yellow ($\lambda_{max} = 526$ nm, PLQY = 1.2%) emissions were observed for PTz-TPB-COF, PTz-BTA-COF, PTz-Py-COF and OPTz-BTA-COF powders in air, respectively (Fig. S20 and Table S11†). The photoluminescence lifetimes were 1.81, 2.13, 1.57, and 0.83 ns (Fig. S21 and Table S11†). We found that the luminescence properties including the emission color, PLQY, and lifetime of PTz-TPB-COF and PTz-Py-COF were variable in solvent environments (Fig. S22, S24 and Table S12†): low-polar solvents such as hexane yielded blue-shifted spectra and suppressed PLQY, whereas medium-polar solvents such as dichloromethane yielded the highest PLQY of 17.6% for PTz-TPB-COF. On the other hand, PTz-BTA-COF and OPTz-BTA-COF showed luminescence properties independent of solvents (Fig. S23, S25 and Table S12†), indicating that the n–π conjugated imine bonds influence the luminescence properties of PTz-TPB-COF and PTz-Py-COF. All four COFs exhibited

outstanding photostability; after irradiation with a white-light Xe lamp (300 W) for 3 h in air, the photoluminescence spectra and PLQY of the COFs remained unchanged (Fig. S26†). High photostability is a prerequisite for efficient photocatalysis.

We further measured the temperature-dependent photoluminescence (TD-PL) spectra to estimate their E_b and elucidate their charge recombination and separation kinetics (Fig. 3).[38] The photoluminescence intensity increased monotonically in all the COF samples as the temperature decreased, which is consistent with other organic semiconductors,[15–17] indicating that the excitons tend to dissociate into charge carriers at high temperature and more readily undergo radiative decay at low temperature because of the freezing of the structural configuration that minimizes the traps and defects.[39] The E_b can be obtained by fitting the temperature dependence of integrated photoluminescence intensity according to the Arrhenius equation, $I(T) = I_0/[1 + A\exp(-E_b/k_BT)]$, where I_0 is the intensity at 0 K, k_B is the Boltzmann constant, and T is the temperature.[38–40] Accordingly, the E_b values for PTz-TPB-COF, PTz-BTA-COF, PTz-Py-COF, and OPTz-BTA-COF were calculated to be 50.4 ± 1.8, 56.8 ± 3.1, 70.6 ± 2.6, and 53.9 ± 3.2 meV, respectively (Fig. 3). To our knowledge, such low E_b values were even comparable with those in strong D–A linear polymers and inorganic materials.[5–9,16,17,41,42] These results clearly demonstrated an effective charge separation process in these phenothiazine-based COFs. The phenothiazine moiety is crucial to reducing the E_b values by constructing the D–A structure and promoting charge separation, even when the acceptor unit is pyrene, commonly recognized as a medium-strong electron donor. On the other hand, OPTz-BTA-COF also exhibited low E_b; this is attributed to the strong cyano groups as strong electron acceptors that also constructed efficient D–A charge-separation systems in the COF lattice.

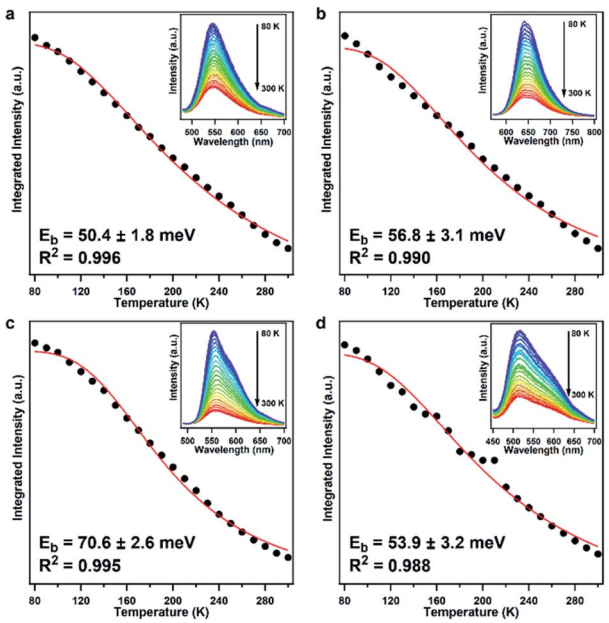

Fig. 3 Integrated photoluminescence intensity as a function of temperature from 80 to 300 K of (a) PTz-TPB-COF, (b) PTz-BTA-COF, (c) PTz-Py-COF, and (d) OPTz-BTA-COF. The red curves represent the fitting by using the Arrhenius equation. The inset is the temperature-dependent photoluminescence spectra for each COF.

As a control experiment, we synthesized three TPB and Py-based COFs, namely, TPB-1P-COF, Py-BTA-COF, and Py-1P-COF according to the literature reports (Fig. S27†).[33,34] Unfortunately, TPB-1P-COF did not show any photoluminescence, and we were not able to record its photoluminescence spectra. We measured the TD-PL spectra of Py-BTA-COF and Py-1P-COF and calculated their E_b according to the Arrhenius equation. The E_b values of Py-BTA-COF and Py-1P-COF were 121.9 ± 2.0 and 156.8 ± 1.9 meV (Fig. S28†), which were clearly larger than those of the phenothiazine-based COFs. Therefore, strong D–A structures were essential for constructing low-E_b COFs. Another control experiment was realized by synthesizing amorphous conjugated microporous polymers (CMPs) with the same monomer components as the phenothiazine-based COFs. The three polymers, namely, PTz-TPB-CMP, PTz-BTA-CMP, and PTz-Py-CMP, were subjected to the TD-PL measurements for E_b evaluation. The E_b values of PTz-TPB-CMP, PTz-BTA-CMP, and PTz-Py-CMP were 77.3 ± 3.0, 79.7 ± 1.3, and 85.8 ± 3.5 meV (Fig. S29†), which were larger than those of the corresponding COFs. Therefore, the ordered packing structure of COFs is also helpful for decreasing the E_b values. All the results demonstrated that both strong D–A structures and ordered packing were key to achieving low-E_b COFs.

To demonstrate the utility of such photoactive, stable, and porous COFs,[43,44] we tested them as photocatalysts in the polymerization reaction, where polymethyl methacrylate (PMMA) was synthesized from methyl methacrylate (MMA) by using ethyl α-bromophenylacetate (EBP) as the initiator and a white-light Xe lamp (300 W) for irradiation in *N*,*N*-dimethylacetamide (DMA) solvent (Table 1). The proposed mechanism of such polymerization is recognized as follows.[45,46] Upon light irradiation, the photocatalyst harvests incident photons and forms excitons, which migrate and dissociate into electrons and holes that react with the initiator. Consequently, the initiator reaches a new electronic state, which decomposes to form a propagating radical and a halide ion Br^-, with the former becoming polymeric and increasing its chain length after MMA monomer addition. After a certain number of monomer additions to the propagating radical, the photocatalyst with positive ions encounters the propagating radical to oxidize it and afford a dormant polymer chain. Based on this mechanism, we first optimized the polymerization conditions, including the ratio of MMA, EBP, and the catalyst, and the reaction time. We fixed a condition in which the ratio of MMA, EBP, and the catalyst was 1000 : 10 : 1 (mol%) and the reaction time was 9 h (Table 1, entries 2–6, Fig. S31–S35†). The weight-average molecular weights (M_w) of PMMA produced by PTz-TPB-COF and PTz-Py-COF were 37.4 and 23.9 kDa (Table 1, entries 2 and 8, Fig. S31 and S37†), respectively, suggesting that the M_w was related to the E_b values and the D–A strength in COFs. However, the partial p–π conjugation in the imine linkage impedes the carrier migration process, resulting in inferior photocatalytic performance. By contrast, the cyanovinylene-linked PTz-BTA-COF showed much-improved performance with a M_w of 176.0 kDa (Table 1, entry 5 and Fig. S34†), whereas OPTz-BTA-COF

Table 1 Results for the photocatalyzed polymerization of MMA catalyzed using a Xe lamp

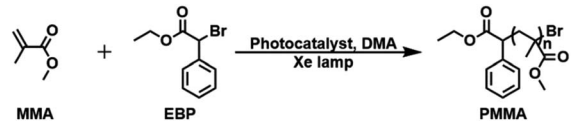

Entry	Photocatalyst	[MMA] : [EBP] : [catalyst] (mol%)	Time (hour)	Conversion (%)	M_n (kDa)	M_w (kDa)	$Đ$ (M_w/M_n)
1	MPTz	[1000] : [10] : [1]	9	19.8	13.6	18.2	1.34
2	PTz-TPB-COF	[1000] : [10] : [1]	9	17.4	21.5	37.4	1.74
3	PTz-TPB-COF	[1000] : [10] : [10]	21	16.8	25.2	61.5	2.44
4	PTz-BTA-COF	[1000] : [20] : [1]	21	18.8	39.2	96.4	2.46
5	PTz-BTA-COF	[1000] : [10] : [1]	9	22.5	100.4	176.0	1.75
6	PTz-BTA-COF	[1000] : [5] : [1]	9	19.5	184.9	357.7	1.93
7	OPTz-BTA-COF	[1000] : [10] : [1]	9	29.0	301.4	471.1	1.56
8	PTz-Py-COF	[1000] : [10] : [1]	9	21.8	13.9	23.9	1.72
9	Py-BTA-COF	[1000] : [10] : [1]	9	26.0	87.9	188.0	2.14
10	Py-1P-COF	[1000] : [10] : [1]	9	4.6	19.7	42.6	2.16
11	PTz-TPB-CMP	[1000] : [10] : [1]	9	31.0	34.9	62.9	1.80
12	PTz-BTA-CMP	[1000] : [10] : [1]	9	32.5	113.6	223.9	1.97
13	PTz-Py-CMP	[1000] : [10] : [1]	9	20.2	73.7	177.6	2.41

exhibited the best performance in producing PMMA with the highest M_w of 471.1 kDa (Table 1, entry 7 and Fig. S36†). OPTz-BTA-COF possessed decreased HOMO and increased LUMO positions and an enlarged bandgap, which were equally critical in the light-induced charge-transfer process to form a strong driving force. To our knowledge, this M_w is remarkably high among the photocatalytic polymerizations (Table S13†). Unlike many photocatalyzed polymerizations that need metal cocatalysts, our catalytic reaction is free of the need for any additional metal catalyst, thus providing new insight for developing a strong D–A structure with low E_b in COFs that substantially promoted the photocatalytic performance. By contrast, the monomer MPTz-based catalyst showed inferior performance with a M_w of only 18.2 kDa (Table 1, entry 1, and Fig. S30†). IR spectra confirmed the structural intactness after the reaction (Fig. S38–S41†), although a few residual PMMA remained in the pores. The COFs remained crystalline after the polymerization (Fig. S42†). The conversion related to the contact of the photocatalyst and the reactant was not high, but it could be improved by decreasing the COF particle size or developing well-dispersed COF materials. Additionally, both applying very low amounts of COF photocatalyst and using light of lower energy are critically important for low-cost and energy-saving production of polymers under mild conditions.

As a control experiment, we performed photocatalytic polymerization by using traditional COF photocatalysts which did not contain phenothiazine. Py-BTA-COF and Py-1P-COF showed a M_w of 188.0 and 42.6 kDa (Table 1, entries 9 and 10, Fig. S43 and S44†), similar to those of PTz-BTA-COF and PTz-Py-COF; however, their $Đ$ values were much increased. Another control experiment by employing amorphous CMPs as photocatalysts was also conducted (Table 1, entries 11–13, and Fig. S45–S47†). Although amorphous CMPs also exhibited photocatalytic polymerization performance with acceptable M_w, they yielded considerably higher $Đ$ compared to the crystalline COFs, indicating that the crystallinity and phenothiazine linkage are keys to achieving polymers with high M_w and low $Đ$. Our results indicated that the rational control of E_b by tailoring the local structure could regulate the charge-transfer process, thereby improving the photocatalytic performance of D–A COF photocatalysts.

Conclusions

In summary, we have constructed four crystalline, porous, and robust phenothiazine-based COFs as a platform for investigating their E_b and photocatalysis. For the first time, phenothiazine as a strong electron donor was incorporated into COF synthesis, which exhibited diverse structures and dimensionalities, the feasibility of bandgap engineering, and low E_b values of 50 meV in COFs. As a demonstration, the polymerization reaction catalyzed by these low-E_b COFs exhibited a remarkably high M_w of 471.1 kDa. We expect that our strategy of D–A type and low E_b COFs could arouse interest in constructing COFs with other strong D/A building blocks for various photochemical applications.

Author contributions

C. G. conceived the project and directed the research. W. W. conducted the synthesis and characterization experiments. H. W. explored the synthetic condition of the COFs. X. T. measured photoluminescence spectra and analyzed the data. J. H. conducted GPC measurements. Y. S. measured N_2 sorption and PXRD. C. L. performed CV measurements. Y. Z. directed photocatalytic experiments. H. X. performed structural modeling. All authors contributed to the writing and editing of the manuscript. W. W. and H. W. contributed equally to this work.

Conflicts of interest

There are no conflicts to declare.

Acknowledgements

This work was supported by the National Natural Science Foundation of China (no. 21975078, 52073161, and 52073089), the Guangdong Basic and Applied Basic Research Foundationgs1: (2021A1515010311), the Natural Science Foundation of Guangdong Province (2019B030301003), the 111 Project (BP0618009), and the Thousand Youth Talents Plan. Y. Su acknowledges the scholarship support from the China Scholarship Council (202006150059). Y. Zhang acknowledges the funding support by the Natural Science Foundation of Zhejiang Province (LZ20E030001). Hong Xu acknowledges the support from the Tsinghua University-Zhangjiagang Joint Institute for Hydrogen Energy and Lithium-Ion Battery Technology.

Notes and references

1 A. Fujishima and K. Honda, *Nature*, 1972, **238**, 37.
2 Z. Jiang, X. Xu, Y. Ma, H. S. Cho, D. Ding, C. Wang, J. Wu, P. Oleynikov, M. Jia, J. Cheng, Y. Zhou, O. Terasak, T. Peng, L. Zan and H. Deng, *Nature*, 2020, **586**, 549.
3 Y. Meng, Y. Luo, J.-L. Shi, H. Ding, X. Lang, W. Chen, A. Zheng, J. Sun and C. Wang, *Angew. Chem., Int. Ed.*, 2020, **59**, 3624.
4 K. Wang, X. Kang, C. Yuan, X. Han, Y. Liu and Y. Cui, *Angew. Chem., Int. Ed.*, 2021, **60**, 19466.
5 A. Alemu, B. Gil and M. Julier, *Phys. Rev. B: Condens. Matter Mater. Phys.*, 1998, **57**, 3761.
6 S. Sun, T. Salim, N. Mathews, M. Duchamp, C. Boothroyd, G. Xing, T. C. Sum and Y. M. Lam, *Energy Environ. Sci.*, 2014, **7**, 399.
7 A. Miyata, A. Mitioglu, P. Plochocka, O. Portugall, J. T.-W. Wang, S. D. Stranks, H. J. Snaith and R. J. Nicholas, *Nat. Phys.*, 2015, **11**, 582.
8 R. Kaupmees, H.-P. Komsa and J. Krustok, *Phys. Status Solidi B*, 2019, **256**, 1800384.
9 M. Baranowski and P. Plochocka, *Adv. Energy Mater.*, 2020, **10**, 1903659.
10 V. I. Arkhipov and H. Bässler, *Phys. Status Solidi*, 2004, **201**, 1152.
11 S. Few, J. M. Frost and J. Nelson, *Phys. Chem. Chem. Phys.*, 2015, **17**, 2311.
12 J. Miao and F. Zhang, *Laser Photonics Rev.*, 2019, **13**, 1800204.
13 Y. Xie and H. Wu, *Mater. Today Adv.*, 2020, **5**, 100048.
14 H. Wang, S. Jin, X. Zhang and Y. Xie, *Angew. Chem., Int. Ed.*, 2020, **59**, 22828.
15 J. Tao, D. Liu, Z. Qin, B. Shao, J. Jing, H. Li, H. Dong, B. Xu and W. Tian, *Adv. Mater.*, 2020, **32**, 1907791.
16 Z.-A. Lan, G. Zhang, X. Chen, Y. Zhang, K. A. I. Zhang and X. Wang, *Angew. Chem., Int. Ed.*, 2019, **58**, 10236.
17 Z.-A. Lan, M. Wu, Z. Fang, X. Chi, X. Chen, Y. Zhang and X. Wang, *Angew. Chem., Int. Ed.*, 2021, **60**, 16355.
18 Y. Dong, H. Cha, H. L. Bristow, J. Lee, A. Kumar, P. S. Tuladhar, I. McCulloch, A. A. Bakulin and J. R. Durrant, *J. Am. Chem. Soc.*, 2021, **143**, 7599.
19 H. Geng, X. Zheng, Z. Shuai, L. Zhu and Y. Yi, *Adv. Mater.*, 2015, **27**, 1443.
20 L. Guo, J. Gong, C. Song, Y. Zhao, B. Tan, Q. Zhao and S. Jin, *ACS Energy Lett.*, 2020, **5**, 1300.
21 A. P. Côté, A. I. Benin, N. W. Ockwig, M. O'Keffe, A. J. Matzger and O. M. Yaghi, *Science*, 2005, **310**, 1166.
22 H. Wang, H. Wang, Z. Wang, L. Tang, G. Zeng, P. Xu, M. Chen, T. Xiong, C. Zhou, X. Li, D. Huang, Y. Zhu, Z. Wang and J. Tang, *Chem. Soc. Rev.*, 2020, **49**, 4135.
23 F. Auras, L. Ascherl, A. H. Hakimioun, J. T. Margraf, F. C. Hanusch, S. Reuter, D. Bessinger, M. Döblinger, C. Hettstedt, K. Karaghiosoff, S. Herbert, P. Knochel, T. Clark and T. Bein, *J. Am. Chem. Soc.*, 2016, **138**, 16703.
24 E. L. Spitler, J. W. Colson, F. J. Uribe-Romo, A. R. Woll, M. R. Giovino, A. Saldivar and W. R. Dichtel, *Angew. Chem., Int. Ed.*, 2012, **51**, 2623.
25 H. Li, P. Shao, S. Chen, G. Li, X. Feng, X. Chen, H.-J. Zhang, J. Lin and Y.-B. Jiang, *J. Am. Chem. Soc.*, 2020, **142**(8), 3712.
26 R. Chen, J.-L. Shi, Y. Ma, G. Lin, X. Lang and C. Wang, *Angew. Chem., Int. Ed.*, 2019, **58**, 6430.
27 N. Keller, T. Sick, N. N. Bach, A. Koszalkowski, J. M. Rotter, D. D. Medina and T. Bein, *Nanoscale*, 2019, **11**, 23338.
28 D. Bessinger, K. Muggli, M. Beetz, F. Auras and T. Bein, *J. Am. Chem. Soc.*, 2021, **143**(19), 7351.
29 J. Zhao, J. Ren, G. Zhang, Z. Zhao, S. Liu, W. Zhang and L. Chen, *Chem.–Eur. J.*, 2021, **27**, 10781.
30 L. Yao, S. Zhang, R. Wang, W. Li, F. Shen, B. Yang and Y. Ma, *Angew. Chem., Int. Ed.*, 2014, **53**, 2119.
31 Y. Lu, H. Song, X. Li, H. Ågren, Q. Liu, J. Zhang, X. Zhang and Y. Xie, *ACS Appl. Mater. Interfaces*, 2019, **11**, 5046.
32 S. M. Sartor, C. H. Chrisman, R. M. Pearson, G. M. Miyake and N. H. Damrauer, *J. Phys. Chem. A*, 2020, **124**, 817.
33 T. Sick, J. M. Rotter, S. Reuter, S. Kandambeth, N. N. Bach, M. Döblinger, J. Merz, T. Clark, T. B. Marder, T. Bein and D. D. Medina, *J. Am. Chem. Soc.*, 2019, **141**, 12570.
34 L. Ascherl, E. W. Evans, M. Hennemann, D. D. Nuzzo, A. G. Hufnagel, M. Beetz, R. H. Friend, T. Clark, T. Bein and F. Auras, *Nat. Commun.*, 2018, **9**, 3802.
35 C. Gu, N. Hosono, J.-J. Zheng, Y. Sato, S. Kusaka, S. Sakaki and S. Kitagawa, *Science*, 2019, **363**, 387.
36 Y. Su, Y. Wan, H. Xu, K.-i. Otake, X. Tang, L. Huang, S. Kitagawa and C. Gu, *J. Am. Chem. Soc.*, 2020, **142**, 13316.
37 C. Zhao, C. S. Diercks, C. Zhu, N. Hanikel, X. Pei and O. M. Yaghi, *J. Am. Chem. Soc.*, 2018, **140**, 16438.
38 M. Gal, Z. Y. Xu, F. Green and B. F. Usher, *Phys. Rev. B: Condens. Matter Mater. Phys.*, 1990, **43**, 1546.
39 S. Lin, H. He, Z. Ye, B. Zhao and J. Huang, *J. Appl. Phys.*, 2008, **104**, 114307.
40 B. Stevens and M. I. Ban, *Trans. Faraday Soc.*, 1964, **60**, 1515.
41 G. Li, P. Fu, Q. Yue, F. Ma, X. Zhao, S. Dong, X. Han, Y. Zhou and J. Wang, *Chem. Catal.*, 2022, DOI: **10.1016/j.checat.2022.05.002**.
42 S. Chai, X. Chen, X. Zhang, Y. Fang, R. S. Sprick and X. Chen, *Environ. Sci.: Nano*, 2022, DOI: **10.1039/d2en00135g**.
43 Y. Qian, D. Li, Y. Han and H.-L. Jiang, *J. Am. Chem. Soc.*, 2020, **142**, 20763.
44 Y.-N. Gong, W. Zhong, Y. Li, Y. Qiu, L. Zheng, J. Jiang and H.-L. Jiang, *J. Am. Chem. Soc.*, 2020, **142**, 16723.
45 J. C. Theriot, C.-H. Lim, H. Yang, M. D. Ryan, C. B. Musgrave and G. M. Miyake, *Science*, 2016, **352**, 1082.
46 A. Jati, K. Dey, M. Nurhuda, M. A. Addicoat, R. Banerjee and B. Maji, *J. Am. Chem. Soc.*, 2022, **144**, 7822.